Journal of Computer-Aided Molecular Design **18:** 719–738, 2004.
DOI 10.1007/s10822-004-7610-1

Conformational analysis of methylphenidate: comparison of molecular orbital and molecular mechanics methods

Kathleen M. Gilbert[a], William J. Skawinski[a], Milind Misra[a], Kristina A. Paris[a], Neelam H. Naik[a], Ronald A. Buono[a], Howard M. Deutsch[b] & Carol A. Venanzi[a,*]
[a]*Department of Chemistry and Environmental Science, New Jersey Institute of Technology, 323 King Blvd., Newark, NJ 07102, USA;* [b]*School of Chemistry and Biochemistry, Georgia Institute of Technology, Atlanta, GA 30332-0400, USA*

Received 18 September 2004; accepted in revised form 13 December 2004

Key words: ab initio, AM1/SM5.4, cocaine, conformational analysis, dopamine, grid search, Hartree-Fock, methylphenidate, molecular mechanics, molecular orbital, random search, solvation, Tripos force field

Summary

Methylphenidate (MP) binds to the cocaine binding site on the dopamine transporter and inhibits reuptake of dopamine, but does not appear to have the same abuse potential as cocaine. This study, part of a comprehensive effort to identify a drug treatment for cocaine abuse, investigates the effect of choice of calculation technique and of solvent model on the conformational potential energy surface (PES) of MP and a rigid methylphenidate (RMP) analogue which exhibits the same dopamine transporter binding affinity as MP. Conformational analysis was carried out by the AM1 and AM1/SM5.4 semiempirical molecular orbital methods, a molecular mechanics method (Tripos force field with the dielectric set equal to that of vacuum or water) and the HF/6-31G* molecular orbital method in vacuum phase. Although all three methods differ somewhat in the local details of the PES, the general trends are the same for neutral and protonated MP. In vacuum phase, protonation has a distinctive effect in decreasing the regions of space available to the local conformational minima. Solvent has little effect on the PES of the neutral molecule and tends to stabilize the protonated species. The random search (RS) conformational analysis technique using the Tripos force field was found to be capable of locating the minima found by the molecular orbital methods using systematic grid search. This suggests that the RS/Tripos force field/vacuum phase protocol is a reasonable choice for locating the local minima of MP. However, the Tripos force field gave significantly larger phenyl ring rotational barriers than the molecular orbital methods for MP and RMP. For both the neutral and protonated cases, all three methods found the phenyl ring rotational barriers for the RMP conformers/invertamers (denoted as cte, tte, and cta) to be: cte, tte > MP > cta. Solvation has negligible effect on the phenyl ring rotational barrier of RMP. The B3LYP/6-31G* density functional method was used to calculate the phenyl ring rotational barrier for neutral MP and gave results very similar to those of the HF/6-31G* method.

Abbreviations: AM1 – Austin Model; SM5.4 – Solvent Model, parameterization 5.4; MP – methylphenidate; RMP – rigid methylphenidate; nMP – neutral methylphenidate; pMP – protonated methylphenidate; nRMP – neutral rigid methylphenidate; pRMP – protonated rigid methylphenidate; QSAR – quantitative structure-activity relationships; RMSD – root mean square deviation; RS – random search; SAR – struc-

*To whom correspondence should be addressed. Fax: +1-973-596-3596; E-mail: venanzi@adm.njit.edu

ture-activity relationships; CoMFA – Comparative Molecular Field Analysis; DAT – dopamine transporter; PES – potential energy surface; HF/6-31G* – Hartree-Fock 6-31G* basis set. For the RMP notations: cte (ring *c*is, *t*rans stereochemistry, phenyl group *e*quatorial), tte (ring *t*rans, *t*rans stereochemistry, phenyl group *e*quatorial), and cta (ring *c*is, *t*rans stereochemistry, phenyl group *a*xial).

Introduction

The 'dopamine hypothesis' [1] implicates the dopamine transporter (DAT) in cocaine abuse and addiction. Structure–activity relationship (SAR) studies for several classes of dopamine reuptake inhibitors such as those that have been recently reviewed [2–5] provide a wealth of data for pharmacophore modeling. In particular Comparative Molecular Field Analysis [6] (CoMFA), Quantitative Structure-Activity Relationship Studies (QSAR), and molecular modeling have been carried out on various classes of dopamine reuptake inhibitors such as tropanes [7–19], piperidine-based cocaine analogues [20], benztropine [21, 22], BTCP [23], bupropion [24], mazindol [25], GBR 12909 analogues [26], and novel piperadinols [27].

Because of the similarity of its mechanism of action to that of cocaine, combined with its limited abuse potential, there has been considerable interest in methylphenidate (Ritalin®; MP; Figure 1a) and its analogues [28–41]. A wide range of MP SAR studies have been produced by the Deutsch and Schweri laboratories [42–53] including the identification of a rigid MP analogue (RMP; Figure 1b) which has the same DAT binding affinity as MP [54]. Additional MP SAR studies have been carried out by other laboratories [55, 56]. Some pharmacophore modeling has been carried out on methylphenidate in an attempt to relate its activity to tropane-based dopamine reuptake inhibitors [57].

Although there is considerable evidence that many ligands do not bind to proteins in their vacuum phase global energy minimum (GEM) conformation [58–62], many pharmacophore models of dopamine reuptake inhibitors have been based on the GEM structure of the ligand, or on a few structures very close in energy to the GEM [11, 25, 26]. Since CoMFA is notoriously sensitive to the conformation used for the calculation [6, 63], we plan to use representative structures from *each* of the local minima on the conformational PES of MP as templates for a future CoMFA study of MP analogues. Others have shown the importance of considering conformations other than the GEM in pharmacophore modeling [64–69].

The question arises, however, as to how sensitive the identification of minima on the MP conformational PES is to the calculation method employed since this, through the choice of conformation used as a template, may ultimately affect the CoMFA results. Similarly, although the ligand becomes at least partially desolvated upon binding to the transporter protein, it is useful to know to what extent solvent affects the potential energy surface of the molecule. In the present work we probe the features of the conformational PES of MP and RMP. We address the sensitivity of the PES to the calculation method employed by comparing the results obtained using the Tripos vacuum phase force field [70] and the RS conformational analysis technique to those obtained from a systematic grid search in vacuum and solvent phases using the AM1 [71–73], AM1/SM5.4 [74], and HF/6–31G* [75] molecular orbital approaches. We compare the minima located by the systematic grid search technique using these different computational methods to those found by the RS protocol using the Tripos force field. We also compare the phenyl ring rotational barrier calculated by these techniques to that calculated by density functional theory for neutral MP. Since the RMP invertamers essentially 'freeze out' potential binding (or bioactive) conformers of MP, we compare representative structures of both MP and RMP in order to select optimal MP templates for a future CoMFA study of MP analogues.

Methods

State of protonation

Studies of the pH dependence of dopamine binding to the DAT [76] indicate that dopamine most

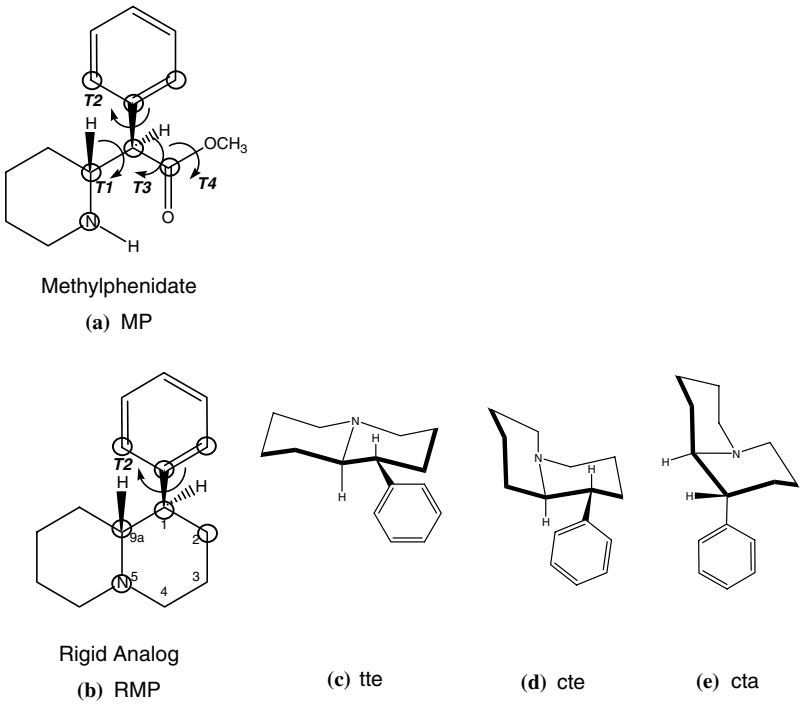

Figure 1. Structures of methylphenidate and rigid methylphenidate.

likely binds in the protonated state. In contrast, similar studies of the cocaine analogue WIN 35,428 [77] indicate that the protonated and neutral species have similar binding affinity. Since it is not clear whether methylphenidate binds to the DAT in the neutral or protonated state or both, calculations were carried out for neutral and protonated methylphenidate (nMP and pMP) and neutral and protonated rigid methylphenidate (nRMP and pRMP). For pMP and pRMP, the added proton was in the axial position.

Selection of molecules

(R,R)-(+)methylphenidate (i.e., (+)-*threo* methylphenidate) was modeled, since it has been identified as the active form of methylphenidate [45]. In this study we focus on the torsional angles T1 and T2 (Figure 1a) which orient two important pharmacophore elements: the quaternary nitrogen and the aromatic ring. These two features were chosen because they are found in most classes of dopamine reuptake inhibitors. This choice is particularly relevant in the case of MP because of the discovery of a rigid analogue, RMP (Figure 1b), which has the same DAT binding affinity as MP and yet only has only these two pharmacophore features. For displacement of the cocaine analogue [^{3}H] WIN 35,428 at the dopamine transporter, IC_{50} (MP) = 84.3 ± 6.3 nM [44] and IC_{50} (RMP) = 84.5 ± 3.5 nM [54]. The nitrogen atom of RMP can invert and is therefore not configurationally stable like carbon. This leads to a more complicated mixture of species, which includes both invertamers (diastereomers) and conformers. There are actually three predicted species of RMP: cta (cis trans axial), cte (cis trans equatorial), and tte (trans trans equatorial). The first term identifies the ring juncture as either *cis* or *trans* (rapid inversion is expected at the nitrogen atom). The second term refers the stereochemistry of the compounds which is always *trans* (analogous here to *threo*). The third term is the conformation of the phenyl group as either axial or equatorial. The neutral species are identified as ncta, ncte, and ntte; the protonated species, by pcte (Figure 1c), ptte (Figure 1d), and pcta (Figure 1e). Note that the species cte and cta are conformers of each other, whereas tte is related to the others by an inversion at N (invertamer or diastereomer). Since RMP restricts the orientation of the important pharmacophore elements in (T1, T2) space and has

the same DAT affinity as MP, this molecule provides important clues to the bioactive conformation of MP.

Calculation of potential energy surfaces and rotational barriers; location of minima

The following calculations were carried out to compare the PES of MP in (T1, T2) space calculated by different methods in vacuum and solvent, to probe the sensitivity of the location of energy minima to calculation technique employed, and to evaluate the effect of solvent on the T2 rotational barriers of MP and RMP. For MP, a vacuum phase grid search was carried out in which torsional angles T1 and T2 were altered in increments (see below) from −180° to 180° for each computational method. The geometry was optimized at each grid point. The grid search was repeated using different solvent approximations (described below) for the molecular mechanics and semiempirical molecular orbital approaches. No solvent calculations were carried out in the *ab initio* molecular orbital case. The PES contour plots were done using the Origin Pro 7, Version 7.0383 (B383) package (available from OriginLab Corporation, Northhampton, MA).

For MP a vacuum phase RS conformational analysis was also carried out using molecular mechanics. The locations of energy minima in (T1, T2) space identified by this technique were compared to those found by the grid searches using the molecular mechanics and molecular orbital methods.

Although comparison of the grids can give an overall impression of the effect of solvent and calculation method on the PES of MP, a more direct comparison was made by calculating the phenyl ring (T2) rotational barrier of MP in the molecular mechanics and semiempirical molecular orbital methods at the ab initio molecular orbital optimized-geometries. A 'slice' was taken through the HF/6–31G* PES at T1 = −60° (near the T1 value of the GEM conformer) in order to provide a set of optimized geometries for the range T2 = 0° to 180° in 30° increments. Single point molecular mechanics and semiempirical molecular orbital calculations in vacuum and solvent were carried out at each of the HF/6–31G*-optimized geometries. The effect of electron correlation on the rotational barrier of nMP was investigated by the use of density functional theory. Single point B3LYP/6–31G* [78] calculations were carried out at each of the HF/6–31G*-optimized geometries.

Similarly for each of the RMP invertamers, the phenyl ring (T2) rotational barrier was calculated with the molecular mechanics and semiempirical molecular orbital methods at the *ab initio* molecular orbital-optimized geometries. T2 was rotated in 30° increments from 0° to 180°, and the geometry was optimized at each new value of T2 using the HF/6–31G* basis set. Single point molecular mechanics and semiempirical molecular orbital calculations in vacuum and solvent were carried out at each of the HF/6–31G*-optimized geometries. The phenyl ring rotational barriers were plotted using Microsoft Excel 98.

In order to analyze the relationship of intramolecular steric effects to the relative conformational energy, the distance between various pairs of nonbonded hydrogens was determined for MP and RMP conformers calculated by the Tripos vacuum phase force field. The minimum H...H distance was plotted for each T2.

The local energy minima conformers of nMP and pMP found by the RS method using the Tripos vacuum phase force field were compared to each other and to those of RMP optimized using the same force field. The structures were superimposed by the atoms indicated by circles in Figures 1a and 1b and the root mean square deviation (RMSD) of all heavy (i.e. non-hydrogen) atomic positions was calculated for each pair of structures.

Molecular mechanics calculations

Both the grid search and random search calculations were carried out using the SYBYL Version 6.9 molecular modeling program (available from Tripos, Inc., St. Louis, MO) with the Tripos [70] force field and Gasteiger–Hückel atomic charges. The dielectric constant parameter, D, was set equal to one for the vacuum phase and 80 for the solvent calculations in the default distance-dependent dielectric function, $D_{dd} = r\ D$, where r is the distance in Ångstroms between two atoms. For MP the 'Aggregates Active' option was used for the piperidine ring, which means the geometry of the ring was held fixed during geometry optimization of the molecule at each (T1, T2) grid point. One thousand iterations of minimization were carried out at each grid point. Grid points were calculated

in 10° increments. Inversion of the piperidine ring was prevented by keeping it as an aggregate. For RMP the 'Aggregates Active' option was used for the quinolizidine ring system.

Random search conformational analysis [79] in vacuum phase was carried out using the four non-ring torsional angles in MP (angles T1, T2, T3, and T4 in Figure 1a). The energy of each randomly generated conformation was minimized using SYBYL's Tripos force field and MAXIMIN2 minimizer with the Powell conjugate-gradient method and a nonbonded distance cutoff of 8.0 Å. Ten thousand search iterations were carried out using an energy cutoff of 20 kcal/mol above the lowest energy conformer found. The energy cutoff was purposely set high in order to thoroughly probe the PES of the molecule for comparison to the grid search results. The RMSD threshold for distinguishing between two conformers was 0.20 Å while the convergence threshold used during the minimization was 0.05. Chirality checking was turned 'On' in order to force the chirality to remain the same during the search.

Semiempirical molecular orbital calculations

Calculations were carried out using the Spartan'02 molecular modeling program (available from Wavefunction, Inc., Irvine, CA) with the AM1 method [71–73] for vacuum phase calculations and AM1/SM5.4 [74] for solvent (water). Grid points were calculated in 10° increments.

Ab initio molecular orbital calculations

Calculations were carried out using the GAUSSIAN98 program [80]. The HF/6–31G* basis set was used for the vacuum phase calculations. No solvent phase calculations were carried out. Grid points were calculated in 30° increments for T1 = −180°–150° and T2 = 0°–150°.

The next section presents the results of the grid search and RS methods applied to MP. Comparison of two-dimensional energy contour plots of the grid search results shows the similarities and differences between the molecular mechanics and molecular orbital methods, as well as the effect of solvation and protonation on the PES. Minima determined by the RS technique (Tripos force field, vacuum phase) are plotted on all the contour maps in order to discern how sensitive the location of the minima may be to calculation method, solvent phase and protonation state. The phenyl ring rotational barriers for MP and RMP are plotted for all three techniques and the effect of solvation phase and protonation state on the rotational barriers is noted.

Results

Methylphenidate: location of minima on the PES

Random search

Figure 2 gives the RS results for neutral and protonated MP. Each RS run took approximately two days on a Silicon Graphics workstation with an R10000 processor running Irix 6.5. In the energy range from 0 to 20 kcal/mol, 67 unique conformers were found for nMP and 28 for pMP. For both the neutral and protonated random searches, every conformer was found at least three times. The probability of finding all possible conformers during the random search is given by [79]:

$$\text{Probability of finding all conformers} = 1-(0.5)^n,$$

where n is the number of times each conformer was found. This suggests that there was approximately an 87.5% chance that all possible conformations were found during each of the two searches. The locations of the minima are plotted in (T1, T2) space in Figure 2. Because rotation of the phenyl ring is symmetric around the torsional angle T2, the same energy is obtained at T2 as at T2 + 180°. This is indicated by the repeating pattern of minima along the T2 axis. Figures 2a and b show that the RS procedure located a wide range of local minima throughout the PES of the molecule.

Figure 2a shows that the nMP energy minima take on almost the full range of T2 values, but are more restricted in their T1 values. In contrast, Figure 2b shows that the pMP minima are more tightly clustered with respect to both T1 and T2. Both nMP and pMP show an approximate three-fold rotational symmetry around the carbon (sp^3)-carbon (sp^3) bond in the T1 torsional angle. The minima are located approximately 120° apart (in 'staggered' conformations) at roughly T1 = ±60° and ±180°. No RS conformers are found in the region of maximum energy, i.e. the 'eclipsed' conformations with T1 = 0° and ±120°. The behavior of MP agrees with the ethane

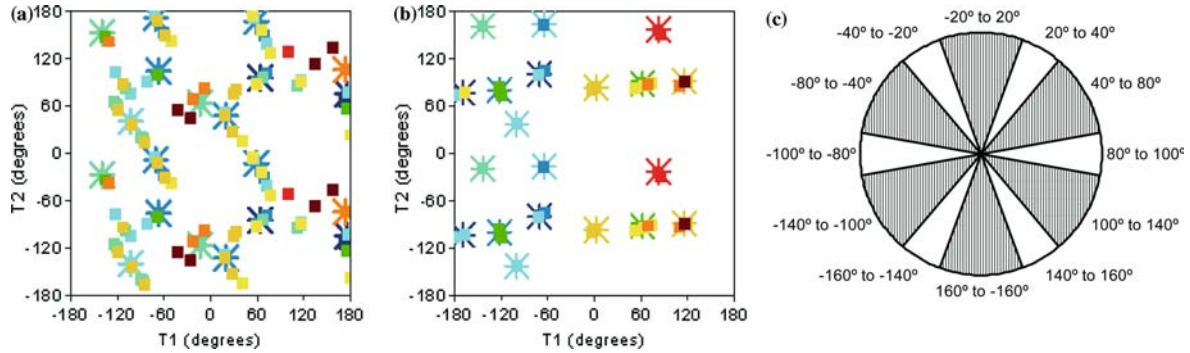

Figure 2. Tripos force field random search results. The points in Figure 2 are color-coded by relative energy (kcal/mol) as follows: Dark blue: 0–2. Blue: 2–4. Light blue: 4–6. Sea green: 6–8. Green: 8–10. Yellow: 10–12. Gold: 12–14. Orange: 14–16. Red: 16–18. Dark red: 18–20+. (a) Torsional angles T1 vs. T2 plot of random search results for neutral MP, (b) protonated MP, (c) sterically favored orientations of substituents on carbon atoms in a $C(sp^3)$–$C(sp^2)$ bond. White (blank) areas are sterically favored, lined areas are sterically unfavored.

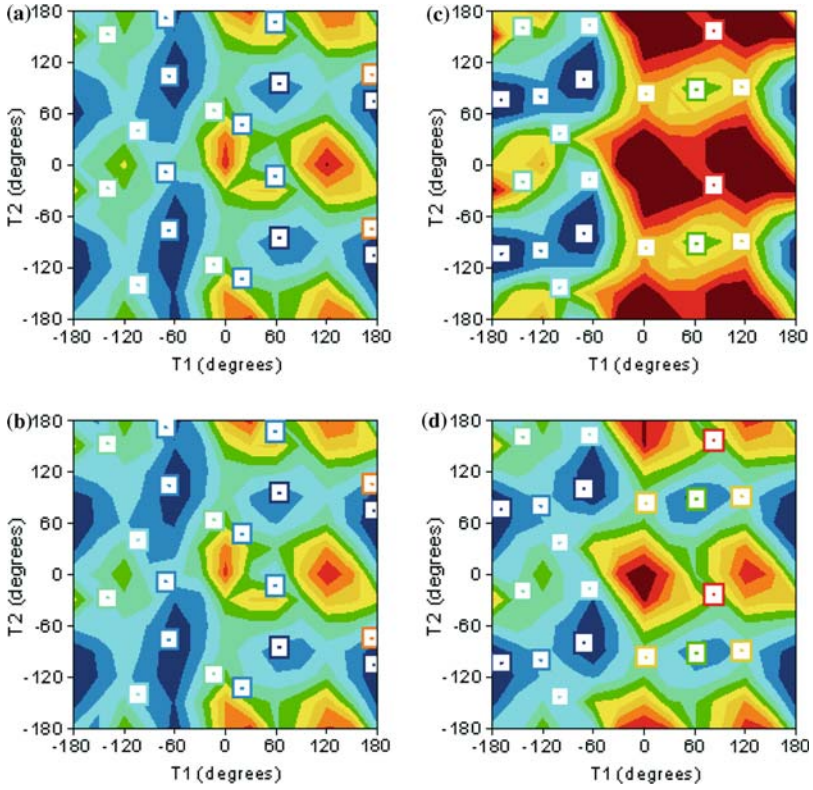

Figure 3. MP potential energy surfaces (Tripos force field). The contours are color-coded by relative energy (kcal/mol) as follows: Dark blue: 0–2. Blue: 2–4. Light blue: 4–6. Sea green: 6–8. Green: 8–10. Yellow: 10–12. Gold: 12–14. Orange: 14–16. Red: 16–18. Dark red: 18–20+. The representative structures (i.e., the conformers indicated by stars in Figures 2a and b) are shown as a white box with a border color-coded by their Tripos vacuum phase force field energy. (a) Potential energy surface of nMP, Tripos force field, vacuum phase, (b) solvent phase, (c) potential energy surface of pMP, Tripos force field, vacuum phase, (d) solvent phase.

rotational barrier (taken as a model of the rotational barrier around a $C(sp^3)$–$C(sp^3)$ bond). Similarly both nMP and pMP show an approximate six-fold rotational symmetry around the $C(sp^3)$–$C(sp^2)$ bond in the T2 torsional angle. The minima occur at approximately $T2 = \pm 30°$,

Table 1. RMSD values for superposition of pairs of representative structures from different clusters, neutral methylphenidate[a].

Cluster[b]	Rel. E.[c]	N1	N2	N3	N4	**N5**	**N6**	N7	N8	**N9**	N10
N1	1.22	0	1.00	1.00	1.19	1.54	1.62	1.71	1.68	1.07	1.44
N2	3.71	1.00	0	0.65	0.94	1.37	1.41	1.23	1.30	1.52	1.24
N3	3.97	1.00	0.65	0	0.38	1.04	1.18	1.13	1.43	1.53	1.49
N4	6.91	1.19	0.94	0.38	0	0.71	0.95	0.94	1.36	1.52	1.44
N5	2.30	1.54	1.37	1.04	0.71	0	0.76	0.73	0.95	1.45	1.18
N6	5.08	1.62	1.41	1.18	0.95	0.76	0	0.58	0.71	1.15	1.10
N7	3.69	1.71	1.23	1.13	0.94	0.73	0.58	0	0.72	1.52	1.28
N8	7.05	1.68	1.30	1.43	1.36	0.95	0.71	0.72	0	1.22	0.79
N9	0	1.07	1.52	1.53	1.52	1.45	1.15	1.52	1.22	0	1.08
N10	14.60	1.44	1.24	1.49	1.44	1.18	1.10	1.28	0.79	1.08	0

[a]RMSD values are average differences in location of all heavy atoms in each molecule, after superposition (see text), in Å.
[b]Representative structure for each cluster of low energy conformers found in the random search.
[c]Relative energy in kcal/mol.

Table 2. RMSD values for superposition of pairs of representative structures from different clusters, protonated methylphenidate[a].

Cluster[b]	Rel. E.[c]	**P1**	P2	**P3**	**P4**	P5	P6	P7	P8	P9	P10
P1	0.66	0	0.51	0.83	1.00	1.31	0.87	1.47	0.76	1.42	1.30
P2	3.28	0.51	0	0.47	0.60	1.01	0.80	1.55	1.14	1.62	1.15
P3	4.21	0.83	0.47	0	0.69	0.70	0.70	1.61	1.37	1.52	1.13
P4	0	1.00	0.60	0.69	0	0.64	0.95	1.37	1.36	1.58	0.82
P5	3.22	1.31	1.01	0.70	0.64	0	0.79	1.49	1.55	1.42	1.11
P6	7.88	0.87	0.80	0.70	0.95	0.79	0	1.67	1.29	1.45	1.48
P7	8.13	1.47	1.55	1.61	1.37	1.49	1.67	0	1.12	1.16	0.89
P8	13.07	0.76	1.14	1.37	1.36	1.55	1.29	1.12	0	1.07	1.11
P9	16.82	1.42	1.62	1.52	1.58	1.42	1.45	1.16	1.07	0	1.31
P10	13.62	1.30	1.15	1.13	0.82	1.11	1.48	0.89	1.11	1.31	0

[a]RMSD values are average differences in location of all heavy atoms in each molecule, after superposition (see text), in Å.
[b]Representative structure for each cluster of low energy conformers found in the random search.
[c]Relative energy in kcal/mol.

Table 3. RMSD values for superposition of pairs of representative structures from different clusters, neutral and protonated methylphenidate[a].

Cluster[b]	**P1**	P2	**P3**	**P4**	P5	P6	P7	P8	P9	P10
N1	1.15	1.35	1.48	1.29	1.470	1.54	0.91	0.54	1.01	0.77
N2	1.54	1.65	1.50	1.55	1.370	1.52	1.15	1.16	0.27	1.18
N3	1.51	1.45	1.36	1.22	1.360	1.65	0.98	1.31	0.84	0.89
N4	1.46	1.27	1.19	1.00	1.250	1.60	1.12	1.46	1.10	0.92
N5	1.34	1.09	1.16	**0.87**	1.010	1.27	1.35	1.63	1.40	1.26
N6	1.02	0.85	**0.79**	1.01	1.130	1.10	1.59	1.51	1.41	1.43
N7	1.41	1.19	0.91	1.12	0.860	1.11	1.70	1.76	1.27	1.47
N8	1.12	1.12	1.03	1.26	1.150	0.85	1.69	1.48	1.20	1.70
N9	**0.19**	0.64	0.93	1.10	1.390	0.94	1.40	0.64	1.40	1.29
N10	1.03	1.24	1.49	1.47	1.540	1.23	1.41	1.19	1.08	1.69

[a]RMSD values are average differences in location of all heavy atoms in each molecule, after superposition (see text), in Å.
[b]Representative structure for each cluster of low energy conformers found in the random search.

$\pm 90°$, and $\pm 150°$. No RS conformers are found in the region of maximum energy, i.e. the 'eclipsed' conformations with $T2 = 0°$, $\pm 60°$, $\pm 120°$, and $\pm 180°$. This behavior agrees with the methylbenzene rotational barrier, a model for rotation around a $C(sp^3)$–$C(sp^2)$ bond. Because of the large substituents on either side of the $C(sp^3)$–$C(sp^2)$ bond in MP, the location of the MP minima is far less precise than described above. Figure 2c shows the approximate six-fold symmetry of low and high energy regions around the $C(sp^3)$–$C(sp^2)$ bond. In the figure the regions of relatively low energy are blank (unlined) and those of relatively high energy are lined. For example, the lined regions correspond to regions of unfavorable steric interactions, such as those found in the eclipsed conformers at $T2 = 0°$, $\pm 60°$, $\pm 120°$, $\pm 180°$. Although a thick line is used in the figure to separate the blank (unlined) and lined regions, in reality the demarcation is far less precise, as shown in Figures 2a and 2b.

The nMP minima in Figure 2a were assigned by inspection to one of 10 clusters based on the similarity of angles T1 and T2 which orient the important pharmacophore elements (phenyl ring and nitrogen). The process was repeated for the pMP minima in Figure 2b. These assignments agreed with the results of hierarchical clustering carried out with SYBYL's clustering tools. The lowest energy conformer in each cluster, indicated by a large star, was taken as the representative structure of that cluster. Tables 1–3 give the results of the RMSD fit of the representative structures of nMP and pMP to themselves and each other. In the tables, N1 stands for the representative structure of nMP cluster 1, P1 for the representative structure of pMP cluster 1, and so on. Table 1 shows that the superposition of each structure with itself gives an RMSD of zero, as expected, and that representative structure i is most similar to representative structure $i + 1$. This is because SYBYL's single-link cluster algorithm orders the structures in terms of similarity and then numbers the clusters accordingly. This means that the numbering of the nMP clusters is unrelated to that of the pMP clusters. Table 3 compares the representative structures of nMP and pMP and shows that, for example, N5 is closest to P4, N6 to P3, and N9 to P1. In Tables 1 and 2 the energy of each MP representative structure in the Tripos vacuum phase force field is given relative to that of its respective GEM structure (i.e. N9 for nMP and P4 for pMP). The tables show that the representative structures span a large energy range. Most are within 7 kcal/mol of the GEM structure.

The locations of these representative structures are also plotted on the MP contour plots in Figures 3–5 below. In this way comparison of the sensitivity of the location of the minima to the calculation method employed can be made.

Grid search

Figures 3–5 show the results of the MP grid searches by the molecular mechanics and molecular orbital methods. Each molecular mechanics grid took about 2 h on a Silicon Graphics Origin 2000 workstation with a 300 MHz processor running Irix 6.5; each semiempirical grid, about 3.5 h on an IBM-compatible personal computer with a 1.01 GHz processor running Windows XP; and each ab initio grid, about 9 h on a Silicon Graphics Origin 3400 workstation with a 400 MHz processor running Irix 6.5. In each grid, the energy is given relative to the GEM conformation for that grid. The range of relative energies for the semiempirical molecular orbital results (0–85 kcal/mol) is much larger than that of the molecular mechanics (0–27 kcal/mol) and ab initio molecular orbital results (0–32 kcal/mol). In order to be able to compare the details of the local minima, which are of more interest than the maxima, the energy was contoured in units of 2 kcal/mol from 0 to 18+ kcal/mol as in Figure 2. However, this means that the highest level (dark red–above 18 kcal/mol) corresponds to 18–85 kcal/mol for the semiempirical results, 18–27 kcal/mol for the molecular mechanics results, and 18–32 kcal/mol for the ab initio results. In each figure the representative structures (i.e. the conformers indicated by stars in Figures 2a and b) chosen from the Tripos RS results are shown as a white box with a border color-coded by their energy calculated in the Tripos vacuum phase force field. Therefore, if a representative structure has the same energy as the contour on which it is located, the border will seem to 'disappear'. Since rotation by 180° around T2 gives a conformer of equal energy, the contour pattern along the T2 axis repeats every 180°. The upper ($T2 = 0°$–$180°$) and lower ($T2 = -180°$–$0°$) portions are the same and are both included in order to have a square grid. This means that each of the 10 representative structures

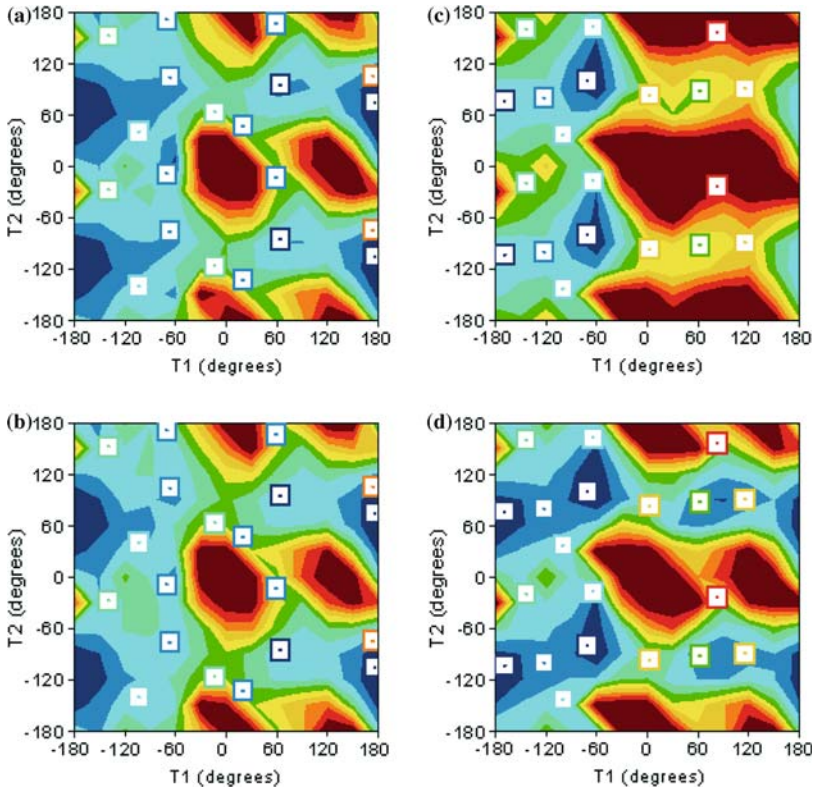

Figure 4. MP potential energy surfaces (AM1 method). The contours are color-coded by relative energy (kcal/mol) as follows: Dark blue: 0–2. Blue: 2–4. Light blue: 4–6. Sea green: 6–8. Green: 8–10. Yellow: 10–12. Gold: 12–14. Orange: 14–16. Red: 16–18. Dark red: 18–20+. The representative structures (i.e., the conformers indicated by stars in Figures 2a and b) are shown as a white box with a border color-coded by their Tripos vacuum phase force field energy. (a) Potential energy surface of nMP, AM1, vacuum phase. (b) Solvent phase. (c) Potential energy surface of pMP, AM1 vacuum phase. (d) Solvent phase.

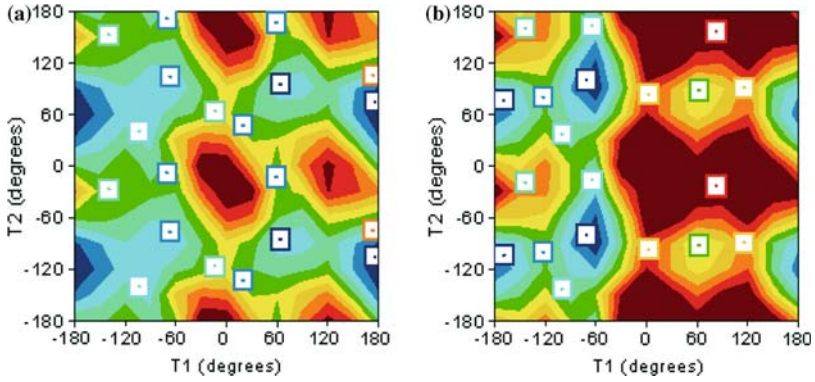

Figure 5. MP potential energy surfaces (HF/6–31G* method). The contours are color-coded by relative energy (kcal/mol) as follows: Dark blue: 0–2. Blue: 2–4. Light blue: 4–6. Sea green: 6–8. Green: 8–10. Yellow: 10–12. Gold: 12–14. Orange: 14–16. Red: 16–18. Dark red: 18–20+. The representative structures (i.e., the conformers indicated by stars in Figures 2a and b) are shown as a white box with a border color-coded by their Tripos vacuum phase force field energy. (a) Potential energy surface of nMP, HF/6–31G*, vacuum phase. (b) Potential enery surface of pMP, HF/6-31G*, vacuum phase.

located at a particular (T1, T2) in the lower portion are repeated at (T1, T2 + 180°) in the upper portion for the sake of completeness. For this reason, the discussion of the RS minima (below) only refers to the minima in the lower (T2 = −180°–0°) portion.

Molecular mechanics calculations Figure 3 gives the results of the MP grid searches in vacuum and solvent using the Tripos force field. The GEM structures are located at the following (T1, T2) grid points; nMP vacuum, Figure 3a: (−60°, −90° or 90°); nMP solvent, Figure 3b: (−60°, −90° or 90°); pMP vacuum, Figure 3c: (−60°, −90° or 90°); and pMP solvent, Figure 3d: (180°, −120° or 60°). Figures 3a–d are qualitatively similar and show that the energy minima are highly localized and that the minima and maxima occur in relatively the same (T1, T2) regions. These regions are determined roughly by the combination of the energy of the eclipsed and staggered conformers in the T1 and T2 torsions. For example, the maxima are found at combinations of the T1 eclipsed conformers at T1 = 0° and ±120° with the T2 eclipsed conformers at T2 = 0°, ±120°, and ±180°. Figure 3a (nMP, vacuum) shows that the highest energy regions are localized in four regions centered approximately at (T1 = 0° and 120°, T2 = 0° and ±180°). Lesser maxima are located at (T1 = 0° and 120°, T2 = ±120°) and (T1 = −120°, T2 = 0°, ±120°, and ±180°).

Similarly the locations of the low energy regions are determined by combinations of the T1 staggered conformers at T1 = ±60° and ±180° with the T2 staggered conformers given in the ranges indicated in Figure 2c. The lowest energy regions are found around (T1 = ±60° and ±180°, T2 = −120° and 60°). Other (T1, T2) staggered conformer combinations result in higher energy. This is typical of all four plots. The MP T2 torsional barrier is discussed in more detail in comparison to the RMP barrier below.

Comparison of Figures 3a and b (nMP, solvent) shows that the effect of solvent (as modeled by setting the dielectric constant to 80) on the nMP PES is negligible. Comparison of Figures 3a and c (pMP, vacuum) shows that the effect of protonation in the vacuum phase is to expand the extent of the high energy regions, destabilizing the minima found at (T1 = 60°, T2 = −120° and 60°) in Figure 3a and truncating the range of the minima located at (T1 = −60° and −180°, T2 = −120° and 60°). Comparison of Figures 3c and d (pMP, solvent) shows that the effect of the simple dielectric solvent model is to significantly stabilize the energy of protonated MP so that the PES resembles that of neutral MP in solvent (Figure 3b).

Figure 3 shows that the RS method correctly identifies the locations of all the minima and appears to pick up additional saddle points. For example, the location of the representative structures in Figures 3a (nMP, vacuum) and 3c (pMP, vacuum) shows that the RS technique correctly locates the three lowest energy minima in the range T2 = −60° to −120° at approximately T1 = −60°, 60°, and ±180°, and gives an additional seven saddle points on the PES. Figures 3b and d show that, since solvent does not affect the location of the three minima, the RS technique with the Tripos vacuum force field correctly identifies the solvent-phase minima.

In Figures 3a and c several of the box borders seem to disappear. This indicates that the energy of the representative structure is the same as that of the surrounding contour. The instances in which a border is of a different color than the surrounding contour are due to the fact that the RS structure for a particular (T1, T2) can differ somewhat from the grid search structure at that (T1, T2) due to a different orientation of the side chain. However, in the solvent case (Figure 3d), the fact that a border is a different color than the surrounding contour at approximately (T1 = 0°, T2 = −100°), (T1 = 60°, T2 = −100°), and (T1 = 120°, T2 = −100°) is due to the fact that solvent has stabilized the energy of the protonated species, lowering the energy of the surrounding contour compared to Figure 3c.

Semiempirical molecular orbital calculations. Figure 4 gives the results of the AM1 MP grid searches in vacuum and solvent. The GEM structures are located at the following (T1, T2) grid points; nMP vacuum, Figure 4a: (180°, −120° or 60°); nMP solvent, Figure 4b: (180°, −120° or 60°); pMP vacuum, Figure 4c: (−60°, −90° or 90°); and pMP solvent, Figure 4d: (−60°, −90° or 90°). Comparison of Figures 4a and b shows that solvent (as approximated by the SM5.4 solvent model) has a negligible effect on the PES of the neutral molecule. Comparison of Figures 4a and c shows that protonation destabilizes the PES surface of the molecule leaving minima localized to only the regions around (T1 = −60°, T2 = −90° and 120°). Comparison of Figures 4c and d shows that solvent stabilizes the PES of the protonated species. The AM1 results are qualitatively similar

to the molecular mechanics results with the minima and maxima occurring in relatively the same regions of (T1, T2) space. In both cases solvent has little effect on the neutral species but stabilizes the protonated species.

Figure 4 shows that the minima identified by the RS technique using the Tripos vacuum phase force field generally agree with the location of the AM1 minima. For example, Figure 4a shows that the RS/Tripos method correctly locates the three lowest AM1 minima at approximately (T1 = 60° and ±180°, T2 = −60° to −120°) and (T1 = −60°, T2 = 0°) for nMP. It correctly identifies three other saddle points near (T1 = 60°, T2 = 0°), (T1 = 0°, T2 = −120°), and (T1 = −140°, T2 = −30°). Similar trends are seen for pMP in Figures 4c and d. In Figures 4a and c about half the boxes have the same color as the surrounding contour, indicating that the Tripos vacuum phase energy is within 2 kcal/mol of the AM1 vacuum phase energy for structures with those particular values of T1 and T2. Cases where the boxes are a different color from the surrounding contour could be due to structures which differ somewhat in their side chain orientations. Large differences in color between the box and the surrounding contour in Figure 4d at approximately (T1 = 0°, T2 = −100°), (T1 = 60°, T2 = −100°), and (T1 = 120°, T2 = −100°) are due to the fact that solvent has stabilized the energy of the protonated species, lowering the energy of the surrounding contour compared to Figure 4c.

Ab initio molecular orbital calculations. Figures 5a and b give the HF/6–31G* results for nMP and pMP, respectively, in vacuum. The GEM structures are located at the following (T1, T2) grid points; nMP vacuum, Figure 5a: (180°, −120° or 60°); and pMP vacuum, Figure 5b: (−60°, −90° or 90°). The figures are qualitatively very similar to the AM1 and molecular mechanics results. Comparison of Figures 5a and b shows that, as in the AM1 case (Figures 4a and c) and the molecular mechanics case (Figures 3a and c), the effect of protonation in vacuum is to extend the high energy regions. The lowest energy contours of pMP are found in two teardrop-shaped regions around (T1 = −60°, T2 = ±90°), and in two regions at (T1 = ±180°, T2 = −120° and 60°). As with the semiempirical and molecular mechanics results, protonation in vacuum appears to limit the range of (T1, T2) space available to the lowest energy MP conformers.

Figure 5 shows that the RS technique with the Tripos vacuum phase force field is able to identify the same minima as the HF/6–31G* method. Figure 5a shows that the RS technique correctly locates the lowest Hartree–Fock minimum at (T1 = ±180°, T2 = −120°) for nMP. In addition the RS/Tripos method locates the HF/6–31G* saddle points at (T1 = ±20°, T2 = −120°), (T1 = −60° and −140°, T2 = −20°). Figure 5b shows that the RS/Tripos method locates the lowest HF/6–31G* minima at (T1 = 60°, T2 = −60°) and (T1 = ±180°, T2 = −120°), as well as the saddle points at (T1 = −120°, T2 = −120°) and (T1 = 0°, 60°, and 120°, T2 = −100°) for pMP.

In summary, although all three methods differ in the local details of the PES, the qualitative trends are the same for neutral and protonated MP. In vacuum phase, protonation has a distinctive effect in decreasing the regions of (T1, T2) space available to the local conformational minima for positive values of T1. Solvent has little effect on the PES of the neutral molecule and tends to stabilize the protonated species. The RS technique and Tripos vacuum phase force field are capable of locating the minima found by the molecular orbital methods. The RS minima show good coverage of the areas of low energy displayed in the contour plots. This shows that the RS minima include key conformations identified by the grid search method using both molecular mechanics and molecular orbital techniques.

Phenyl ring rotational barriers for MP and RMP

It should be emphasized that the phenyl ring rotational barriers reported here were calculated at the HF/6–31G*-optimized geometries. In contrast to the contour plots shown in Figures 3–5, the structures were not re-minimized using the AM1 method or Tripos force field, nor re-minimized in solvent. Values of the energy and minimum H...H distance at each (T1, T2) point are given in the Supplementary Tables. The purpose of this comparison is to give a qualitative indication of the effect of solvent and calculation technique on the magnitude of the phenyl ring rotational barrier.

Methylphenidate

Figure 6 compares the energy barriers for T2 rotation calculated at the HF/6–31G*-optimized geometries for MP with T1 fixed at −60°. Only Figure 6a includes the results of the B3LYP/6–31G* calculation. Figure 6a gives the vacuum phase results for nMP. All four methods show a broad region of low energy for T2 ranging from 90° to 150°. All four methods show qualitatively the same behavior with a maximum relative energy at T2 = 30°. The molecular orbital methods are in close agreement, giving rotational barriers of 8.3, 7.8 and 7.3 kcal/mol, respectively, for the HF/6–31G*, B3LYP/6–31G*, and AM1 techniques, in contrast to the molecular mechanics barrier of 30 kcal/mol. The distance of closest approach of any two nonbonded hydrogens, H...H (indicated by the dotted line with values read from the scale on the right-hand axis), follows the opposite trend of the energy. (Tables 5 and 6 of the Supplementary Tables list the H...H pairs that correspond to the distances plotted in Figures 6, 7 and 9.) The maximum at T2 = 30° is due to a very close distance of approach (1.7 Å) between the hydrogen at position 2 of the phenyl ring and the hydrogen on the nitrogen. Figure 6b shows that both the crude dielectric solvent model and the AM1/SM5.4 model predict negligible effect of solvent on the phenyl ring rotational barriers of nMP.

These general trends are repeated for pMP as seen in Figures 6c and d. Figure 6c shows a barrier of 43 kcal/mol at T2 = 30° for the molecular mechanics calculation in vacuum with a significantly lower barrier for the molecular orbital methods (9.8 kcal/mol for HF/6–31G*; 7.8 kcal/

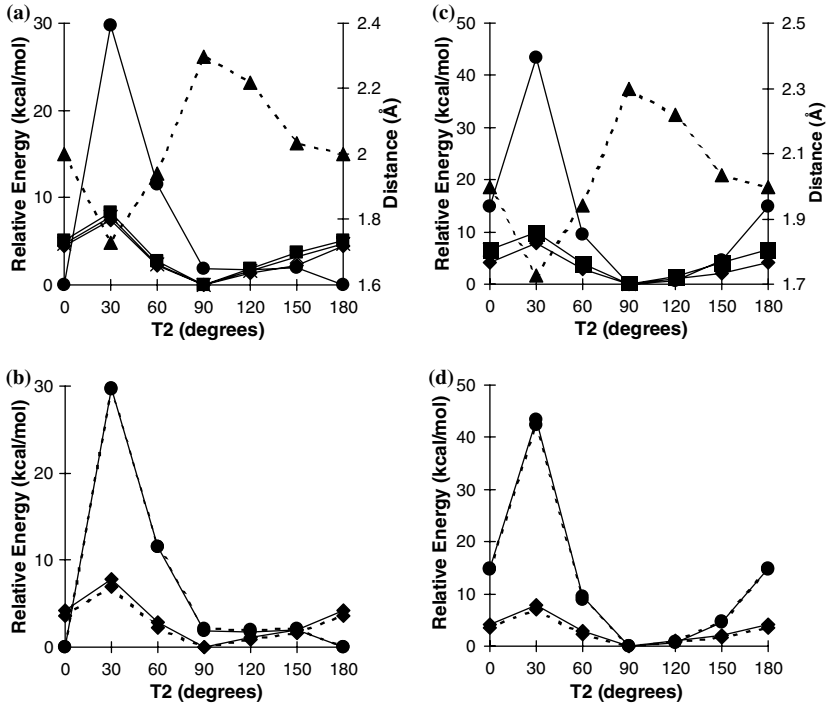

Figure 6. MP phenyl ring rotational barrier. (a) Barrier for nMP, T1 = −60°, method comparison at the HF/6–31G*-optimized geometry, vacuum phase. Solid line, solid square–HF/6–31G* nMP, vacuum; solid line, solid circle–Tripos force field nMP, vacuum; solid line, solid diamond–AM1 nMP, vacuum; solid line, X–B3LYP/6–31G* nMP, vacuum; dashed line, solid triangle–Minimum H...H Distance. (b) Barrier for nMP, T1 = −60°, solvent comparison at the HF/6–31G*-optimized geometry. Solid line, solid circle–Tripos force field nMP, vacuum; dashed line, solid circle–Tripos force field nMP, solvent; solid line, solid diamond–AM1 nMP, vacuum; dashed line, solid diamond–AM1 nMP, solvent. (c) Barrier for pMP at T1 = −60°, method comparison at the HF/6–31G*-optimized geometry, vacuum phase. Solid line, solid square–HF/6–31G* pMP, vacuum; solid line, solid circle–Tripos force field pMP, vacuum; solid line, solid diamond–AM1 pMP, vacuum; dashed line, solid triangle–Minimum H...H Distance. (d) Barrier for pMP at T1 = −60°, solvent comparison at the HF/6–31G*-optimized geometry. Solid line, solid circle–Tripos force field pMP, vacuum; dashed line, solid circle–Tripos force field pMP, solvent; solid line, solid diamond–AM1 pMP, vacuum; dashed line, solid diamond–AM1 pMP, solvent.

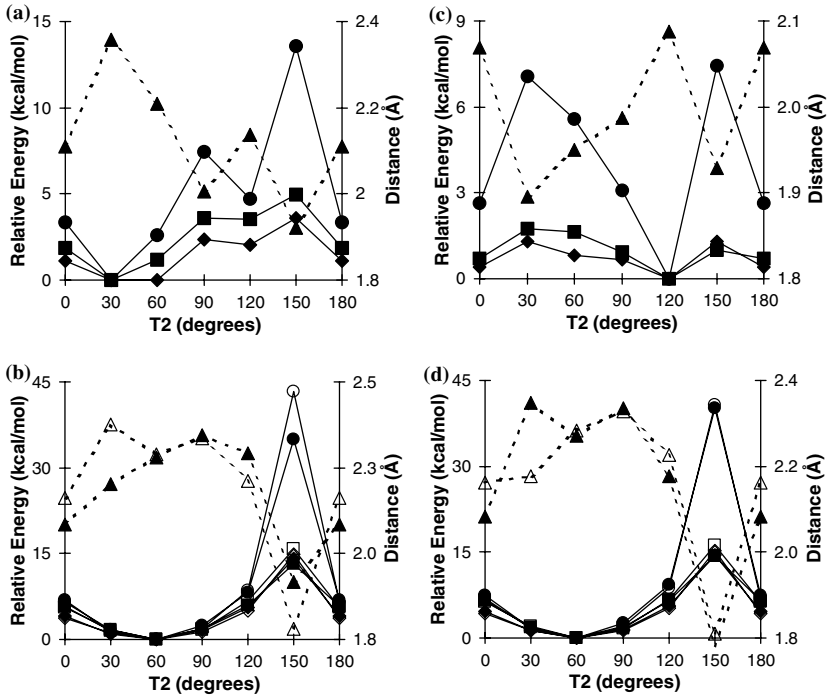

Figure 7. RMP phenyl ring rotational barrier, vacuum. (a) Barrier for ncta, method comparison at the HF/6–31G*-optimized geometry, vacuum phase. Solid line, solid square–HF/6–31G* ncta, vacuum; solid line, solid circle–Tripos force field ncta, vacuum; solid line, solid diamond–AM1 ncta, vacuum; dashed line, solid triangle–Minimum H...H Distance. (b) Barriers for ncte and ntte, method comparison at the HF/6–31G*-optimized geometry, vacuum phase. Solid line, solid square–HF/6–31G* ncte, vacuum; solid line, open square–HF/6–31G* ntte, vacuum; solid line, solid circle–Tripos force field ncte, vacuum; solid line, open circle–Tripos force field ntte, vacuum; solid line, solid diamond–AM1 ncte, vacuum; solid line, open diamond–AM1 ntte, vacuum; dashed line, solid triangle–Minimum H...H Distance, ncte; dashed line, open triangle–Minimum H...H Distance, ntte. (c) Barrier for pcta, method comparison at the HF/6–31G*-optimized geometry, vacuum phase. Solid line, solid square–HF/6–31G* pcta, vacuum; solid line, solid circle–Tripos force field pcta, vacuum; solid line, solid diamond–AM1 pcta, vacuum; dashed line, solid triangle–Minimum H...H Distance. (d) Barriers for pcte and ptte, method comparison at the HF/6–31G*-optimized geometry, vacuum phase. Solid line, solid square–HF/6–31G* pcte, vacuum; solid line, open square–HF/6–31G* ptte, vacuum; solid line, solid circle–Tripos force field pcte, vacuum; solid line, open circle–Tripos force field ptte, vacuum; solid line, solid diamond–AM1 pcte, vacuum; solid line, open diamond–AM1 ptte, vacuum; dashed line, solid triangle–Minimum H...H Distance, pcte; dashed line, open triangle–Minimum H...H Distance, ptte.

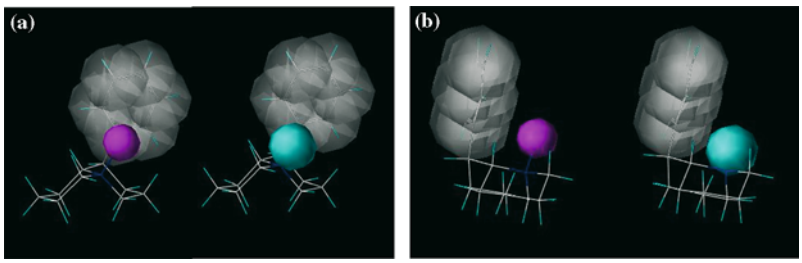

Figure 8. RMP (cta) lone pair and proton orientations. Front view (a) and side view (b) of ncta (left side, pink represents lone pair) and pcta (right side, blue represents hydrogen) energy-minimized structures at T2 = 150°.

mol for AM1). As with nMP, the distance of closest approach of any two nonbonded hydrogens is 1.7 Å. Comparison of Figures 6a and c shows that protonation increases the barrier for T2 rotation in MP by 1.5, 0.4, and 13 kcal/mol for the HF/6–31G*, AM1, and Tripos methods, respec-

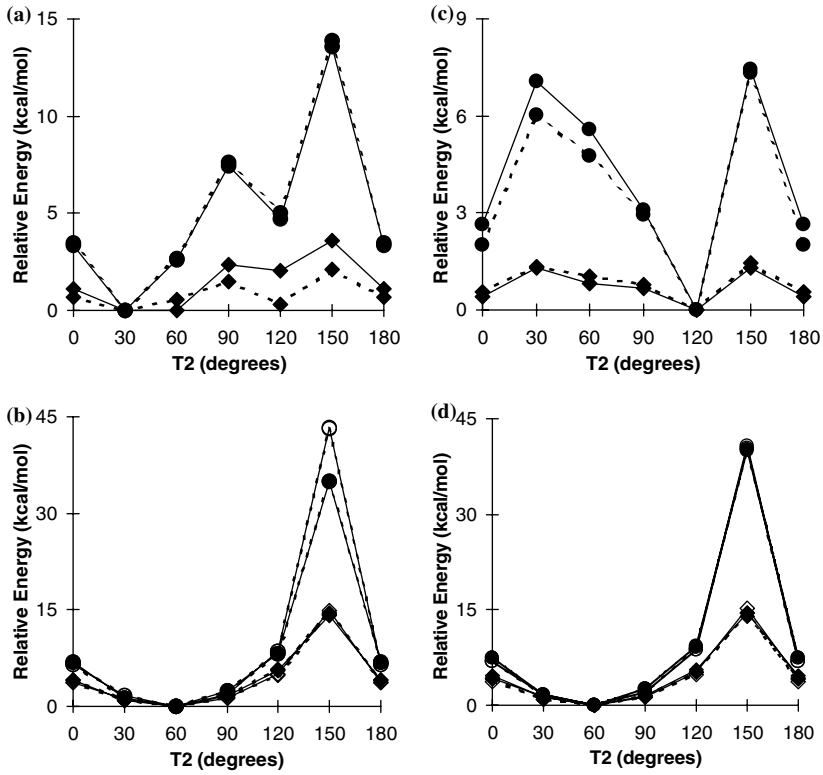

Figure 9. RMP phenyl ring rotational barrier, solvent. (a) Barrier for ncta, solvent comparison at the HF/6–31G*-optimized geometry. Solid line, solid circle–Tripos force field ncta, vacuum; dashed line, solid circle–Tripos force field ncta, solvent; solid line, solid diamond–AM1 ncta, vacuum; dashed line, solid diamond–AM1 ncta, solvent. (b) Barriers for ncte and ntte, solvent comparison at the HF/6–31G*-optimized geometry. Solid line, solid circle–Tripos force field ncte, vacuum; solid line, open circle–Tripos force field ntte, vacuum; dashed line, solid circle–Tripos force field ncte, vacuum; dashed line, open circle–Tripos force field ntte, vacuum; solid line, solid diamond–AM1 ncte, vacuum; solid line, open diamond–AM1 ntte, vacuum; dashed line, solid diamond–AM1 ncte, solvent; dashed line, open diamond–AM1 ntte, solvent. (c) Barrier for pcta, solvent comparison at the HF/6–31G*-optimized geometry. Solid line, solid circle–Tripos force field pcta, vacuum; dashed line, solid circle–Tripos force field pcta, solvent; solid line, solid diamond–AM1 pcta, vacuum; dashed line, solid diamond–AM1 pcta, solvent. (d) Barriers for pcte and ptte, solvent comparison at the HF/6–31G*-optimized geometry. Solid line, solid circle–Tripos force field pcte, vacuum; solid line, open circle–Tripos force field ptte, vacuum; dashed line, solid circle–Tripos force field pcte, vacuum; dashed line, open circle–Tripos force field ptte, vacuum; solid line, solid diamond–AM1 pcte, vacuum; solid line, open diamond–AM1 ptte, vacuum; dashed line, solid diamond–AM1 pcte, solvent; dashed line, open diamond–AM1 ptte, solvent.

tively. Protonation also removes the shallow local minimum (see Supplementary Table 1 for energies) found by the Tripos method at T2 = 120° for nMP, so that pMP has only one minimum located at T2 = 90° for all three methods. Figure 6d shows that solvent has little effect on the pMP rotational barrier.

Rigid methylphenidate analogue

Figure 7 plots the barrier for T2 rotation for the invertamers of neutral and protonated RMP in vacuum at the HF/-6–31G*-optimized geometries in which T1 varies slightly with T2 (see Supplementary Tables). As in the case of MP, the molecular mechanics and molecular orbital methods give qualitatively the same results. The molecular mechanics calculations give a significantly higher rotational barrier than the molecular orbital results, but all three methods give the same conformational energy profile.

In Figure 7a the GEM conformer of ncta is found at (T1 = −79°, T2 = 30°) and a local minimum at (T1 = 82°, T2 = 120°). Global and local maxima are found at (T1 = −75°, T2 = 150°) and (T1 = −86°, T2 = 90°), respectively. The barrier heights at the local maximum are 3.6, 2.3, and 7.4 kcal/mol, respectively, for the HF/6–31G*, AM1, and Tripos methods. At T2 = 90° the dis-

tance of closest approach between any two hydrogens is 2.0 Å between the hydrogen at the 2-position of the phenyl ring and a hydrogen at the 3-position of the quinolizidine ring. The barrier heights at the global maximum are 5.0, 3.6, and 13.6 kcal/mol for the HF/6–31G*, AM1, and Tripos methods, respectively. At T2 = 150° the hydrogen at the 2-position of the phenyl ring is 1.9 Å from the hydrogen on the C9a 'fused' carbon. Comparison of Figures 7a and 6a shows that there is no barrier to rotation at T2 = 30° for ncta. This is because, in contrast to nMP, there is no hydrogen on the ncta nitrogen. Both ncta rotational barriers ((T1 = −86°, T2 = 90°) and (T1 = −75°, T2 = 150°)) are significantly lower than that of nMP at (T1 = −60°, T2 = 30°).

Comparison of Figures 7a and c shows the effect of protonation on the PES of the cta invertamer. The pcta global and local minima are located at (T1 = −77°, T2 = 120°) and (T1 = −74°, T2 = ±180°). The pcta maxima occur at (T1 = −84°, T2 = 30°) and (T1 = −70°, T2 = 150°). The barrier heights at the two maxima are approximately the same: 1.7, 1.3, and 7.1 kcal/mol, respectively, for the HF/6–31G*, AM1, and Tripos methods at (T1 = −84°, T2 = 30) and 1.0, 1.3, and 7.4 kcal/mol for the HF/6–31G*, AM1, and Tripos methods, respectively at (T1 = −70°, T2 = 150°). The pcta maximum at (T1 = −84°, T2 = 30°) is due to the close approach (1.9 Å) between the proton on the nitrogen and the 2-position hydrogen of the phenyl ring. This is similar to the situation seen with nMP and pMP at (T1 = −60°, T2 = 30°), but is very different than ncta which has a minimum at (T1 = −79°, T2 = 30°) due to the fact that there is no hydrogen on the ncta nitrogen. In fact at (T1 = −79°, T2 = 30°), no two hydrogens in ncta approach closer than 2.4 Å.

Comparison of Figures 7a and c shows that both ncta and pcta have a maximum at (T1 = −75°, T2 = 150°) and (T1 = −70°, T2 = 150°), respectively. This is due to the fact that the hydrogen at the 2-position of the phenyl ring and the hydrogen on the C9a 'fused' carbon of the quinolizidine ring are only 1.9 Å apart. However, the rotational barrier for pcta at T2 = 150° is about half that of ncta. The reason for this is shown in Figures 8a and b, which illustrates the relative position of the lone pair and hydrogen with respect to the phenyl ring at T2 = 150° based on the SYBYL default van der Waals radii. The figures show that in ncta the electron cloud of the lone pair is very close to that of the aromatic ring, causing this structure to have higher energy than pcta due to electron–electron repulsion. In pcta the proton is close to the aromatic ring, thereby stabilizing the energy of the pcta conformer.

Comparison of Figures 7c and 6c shows that both pcta rotational barriers at (T1 = −84°, T2 = 30°) and (T1 = −70°, T2 = 150°) are lower than that of pMP at (T1 = −60°, T2 = 30°). This is due in part to the fact that in pcta the closest distance between any two nonbonded hydrogens is only 1.9 Å compared to pMP where this distance is 1.7 Å.

Comparison of Figures 7a and b shows that the ntte and ncte invertamers have a slightly different conformational energy profile and a significantly higher rotational barrier than ncta. Both ntte and ncte have a broad energy minimum region stretching from T2 = 0° to about 120°. The GEM conformer is located at (T1 = 180°, T2 = 60°). The maximum is at (T1 = 175°, T2 = 150°) and is due to the close approach (1.8–1.9 Å) of the 2-position hydrogen of the phenyl ring to the hydrogens at the 2- and 9-positions of the quinolizidine ring for ncte and ntte, respectively. The ncte rotational barriers are 13.3, 14.2 and 35.0 kcal/mol for the HF/6–31G*, AM1, and Tripos methods, respectively. The ntte rotational barriers are 15.9, 14.9, and 43.3 kcal/mol for the HF/6–31G*, AM1, and Tripos methods, respectively. Comparison of Figures 6a, 7a and b shows that in terms of barrier height: ncte, ntte > nMP > ncta for all three methods. In fact the ncte and ntte rotational barriers are about three times as large as the ncta barriers. This trend does not exactly parallel that of the minimum H...H distance which runs from about 1.8–1.9 Å in ncte and ntte to 1.7 Å in nMP to 1.9–2.0 Å in ncta. This is because, as was shown above, other effects such as π cloud-lone pair repulsions come into play.

Comparison of Figures 7b and d shows that protonation has little effect on the rotational barrier and conformational energy profile of the tte and cte invertamers. This is in contrast to the cta invertamer and is due to the fact that the lone pair (in ncte and ntte) and proton (in pcte and ptte) point away from the phenyl ring, whereas in cta they point towards the phenyl ring (Figures 8a and b). The maximum energy is

found at T2 = 150° (T1 = 178° for pcte and 175° for ptte) and is due to the close approach (1.8 Å) of the 2-position hydrogen on the phenyl ring to the 9-position hydrogen on the quinolizidine ring. The pcte rotational barriers are 14.3, 14.6 and 40.3 kcal/mol for the HF/6–31G*, AM1, and Tripos methods, respectively. The ptte rotational barriers are 16.3, 15.2, and 40.6 kcal/mol for the HF/6–31G*, AM1, and Tripos methods, respectively. Comparison to Figures 6c and 7c shows that in terms of barrier height: pcte, ptte > pMP > pcta for all three methods. In fact the pcte and ptte barriers are over five times as large as the pcta barriers. Again this trend does not parallel that of the minimum distance between nonbonded hydrogens, which runs from 1.8 Å in pcte and ptte to 1.7 Å in pMP to 1.9 Å in pcta.

Figure 9 shows the effect of solvent on the T2 rotational barriers of the invertamers of RMP. Neither the crude dielectric model nor the AM1/SM5.4 solvent model significantly affects the barrier height or the conformational energy profile.

Comparison of representative structures of methylphenidate and rigid methylphenidate

Tables 4 and 5 give the RMSD values for the superposition of each MP representative structure with the local energy minimum conformations of each RMP invertamer for the neutral and protonated cases, respectively. The energy of each RMP invertamer in the Tripos vacuum phase force field is given relative to that of its respective GEM structure. The tables show that two minima (ncta1 and ncta2; pcta1 and pcta2) were found for the cta invertamer; only one minimum each was found for cte and tte. For both the nRMP and pRMP invertamers, the tte structure is the GEM. The RMSD values of the best MP/RMP fits are given in bold. The tables show that the best fit between MP and RMP occurs for MP with the cte and tte invertamers (RMSD = 0.1 Å for N9 with ncte and ntte and for P1 with pcte and ptte). Of all the nMP representative structures, N9, the nMP GEM conformer, has the best fit with ntte, the nRMP GEM conformer. Of all the pMP representative

Table 4. RMSD values for superposition of neutral methylphenidate representative structures with neutral rigid methylphenidate invertamers[a].

		Cluster[b]									
RMP	Rel. E.[c]	N1	N2	N3	N4	**N5**	**N6**	N7	N8	**N9**	N10
ncta1	2.01	0.953	0.603	0.677	0.617	0.709	**0.228**	0.317	0.629	0.815	0.984
ncta2	6.68	0.660	0.966	0.721	0.592	**0.202**	0.723	0.520	0.510	0.588	0.569
ncte	1.30	0.759	0.908	0.810	0.787	0.670	0.542	0.923	0.734	**0.119**	0.341
ntte	0	0.761	0.911	0.811	0.786	0.666	0.538	0.921	0.730	**0.117**	0.338

[a]RMSD values are average differences in location of seven key atoms in each molecule, after superposition (see text), in Å.
[b]Representative structure for each cluster of low energy conformers found in the random search.
[c]Relative energy in kcal/mol.

Table 5. RMSD values for superposition of protonated methylphenidate representative structures with protonated rigid methylphenidate invertamers[a].

		Cluster[b]									
RMP	Rel. E.[c]	**P1**	P2	**P3**	**P4**	P5	P6	P7	P8	P9	P10
pcta1	7.99	0.735	0.572	**0.173**	0.754	0.342	0.467	0.975	0.932	0.611	0.921
pcta2	8.32	0.488	0.369	0.702	**0.219**	0.519	0.587	0.650	0.629	0.929	0.575
pcte	2.49	**0.124**	0.351	0.569	0.644	0.954	0.765	0.727	0.495	0.868	0.816
ptte	0	**0.092**	0.357	0.619	0.628	0.904	0.734	0.698	0.449	0.920	0.805

[a]RMSD values are average differences in location of seven key atoms in each molecule, after superposition (see text), in Å.
[b]Representative structure for each cluster of low energy conformers found in the random search.
[c]Relative energy in kcal/mol.

structures, P1, which is only 0.66 kcal/mol higher in energy than the pMP GEM conformer, has the best fit with ptte, the pRMP GEM conformer. Table 5 also shows a very good fit (RMSD = 0.2 Å) for the pMP GEM conformer, P4, with pcta2.

Since RMP is a very rigid molecule and yet has the same binding affinity as MP, it contains part of the pharmacophore for binding 'frozen' into a relatively rigid orientation. It is not possible to separate the invertamers and test their binding affinity, so there is no direct approach to determining the bioactive conformer.

Discussion

The objective of this work was to test the sensitivity of the PES of MP and RMP to calculation method, protonation state, and solvent correction in order to identify conformational energy minima to be used as input templates for CoMFA studies. Calculations were carried out for MP using two-dimensional (T1, T2) grids where the geometry was optimized at each grid point in the HF/6–31G*, AM1, and Tripos methods. Calculations were carried out for neutral and protonated MP in vacuum and solvent. General comparisons were made between the contour plots, but since MP has four rotatable bonds, the optimized HF/6–31G*, AM1, and Tripos structures which have the same (T1, T2) values could differ in the orientation of the side chains. Therefore, direct comparison of rotational barriers could not be made from the contour plots since the molecular structures were not exactly the same. For this reason the T2 rotational barrier was also investigated for MP and RMP in vacuum and solvent using the HF/6–31G*-optimized geometries. This insured that the structures were the same for each method comparison. From these calculations, the following trends were noticed.

Effect of solvent on PES

Solvent was found to have no effect on the T2 rotational barrier of MP or RMP when the structures were frozen in their HF/6–31G*-optimized geometries (see Figures 6, 7 and 9). In contrast, in the contour plots where the structures were allowed to relax their geometries, both solvent models were shown to stabilize the protonated species (see Figures 3–5). It should be noted, however, that the AM1/SM5.4 method carries out the solvent calculation at the AM1 gas-phase-optimized-geometry so that only a correction is added to the gas phase energy. Similarly the Tripos crude dielectric model adds a correction term to the Tripos gas phase energy. Even further stabilization might be noticed with a technique like the Polarizable Continuum Model [81, 82] which allows for geometry optimization in the reaction field of the solvent.

Effect of protonation on PES

The PES contour plots in Figures 3–5 show that the effect of protonation in all three methods is to destabilize the region T1 = 0°–180° for all values of T2. This results in restricting the minima to smaller regions of space in the region T1 = −60° to −180° for all values of T2. All three methods agree in the general location of the minima for both the vacuum and solvent phase. For the T2 rotational barriers calculated at the HF/6–31G*-optimized geometries, the effect of protonation in all three methods is to increase the MP rotational barrier, decrease the cta rotational barrier, alter the cta conformational profile, and to have essentially no effect on the cte and tte barriers. The proton decreases the cta rotational barrier because it points towards the aromatic ring (due to its axial orientation; see Figure 1), stabilizing the energy of the invertamer, in contrast to tte and cte, where the proton points away from the aromatic ring (due to its equatorial orientation).

Effect of calculation method on PES

Comparison of the contour plots in Figures 3–5 indicates that all three methods give qualitatively the same results in terms of the location of the regions of minimum and maximum energy. The Tripos force field gives significantly larger maximum energy values in the T2 rotational barrier study (Figures 6, 7 and 9), where the molecule was frozen in the HF/6–321G*-optimized geometry. In terms of the height of the phenyl ring rotational barriers, all three methods found that cte,

tte > MP> cta for both the neutral and protonated cases, but the Tripos force field gave much higher barriers than the molecular orbital methods. The B3LYP/6–31G* density functional method gave essentially the same barrier as the HF/6–31G* method for nMP.

Comparison of the location of the Tripos RS representative structures to the minima obtained by a comprehensive search of the PES of MP using the molecular mechanics and molecular orbital methods indicates that the RS technique reasonably identifies the locations of the minima. Since the objective is to accurately locate conformational energy *minima* and since all three methods give the same relative location of the lowest energy minima, the Tripos force field used with the RS technique appears to be a very reasonable choice for calculation of local minima. However, the Tripos force field gives exceptionally high phenyl ring rotational barriers when compared to molecular orbital and density functional calculations. Therefore caution should be used in combining it with techniques such as molecular dynamics simulation because the molecule could be trapped in a local minimum due to overestimation of potential energy barriers.

Future work will involve using the MP representative structures in a CoMFA study of MP analogues.

Acknowledgements

This work was supported in part by NIH grant DA11541 (H.M.D. and C.A.V.). K.M.G. acknowledges the support of Ruth L. Kirschstein National Research Service Award Individual Predoctoral Fellowship DA015555. K.A.P. and N.H.N. acknowledge the support of the NJI-TOWER (New Jersey Information-Technology Opportunities for the Workforce, Education, and Research) Undergraduate Research Program, funded by the New Jersey Commission on Higher Education, and the Ronald E. McNair Postbaccalaureate Achievement Program.

References

1. Kuhar, M.J., Ritz, M.C. and Boja, J.W., TINS, 14 (1991) 299.
2. Chen, N.H. and Reith, M.E.A., In Reith, M.E.A. (Ed.), Contemporary Neuroscience: Neurotransmitter Transporters: Structure, Function, and Regulation, Humana Press, Totowa, NJ, 1997, pp. 53–109.
3. Singh, S., Chem. Rev., 100 (2000) 925.
4. Carroll, F.I., J. Med. Chem., 46 (2003) 1775.
5. Prisinzano, T., Rice, K.C., Baumann, M.H. and Rothman, R.B., Curr. Med. Chem. – Central Nervous System Agents, 4 (2004) 47.
6. Cramer, III, R.D., Patterson, D.E. and Bunce, J.D., J. Am. Chem. Soc., 110 (1988) 5959.
7. Carroll, F.I., Gao, Y., Rahman, M.A., Abrams, P., Parham, K., Lewin, A.H., Boja, J.W. and Kuhar, M.J., J. Med. Chem., 34 (1991) 2719.
8. Froimowitz, M., J. Comput. Chem., 14 (1993) 934.
9. Carroll, F.I., Mascarella, S.W., Kuzemko, M.A., Gao, Y., Abraham, P., Lewin, A.H., Boja, J.W. and Kuhar, M.J., J. Med. Chem., 37 (1994) 2865.
10. Yang, B., Wright, J., Eldefrawi, M.E., Pou, S. and MacKerell, Jr., A.D., J. Am. Chem. Soc., 116 (1994) 8722.
11. Lieske, S.F., Yang, B., Eldefrawi, M.E., MacKerell, Jr., A.D. and Wright, J., J. Med. Chem., 41 (1998) 864.
12. Zhu, N., Harrison, A., Trudell, M.L. and Klein-Stevens, C.L., Struct. Chem., 10 (1999) 91.
13. Muszynski, I.C., Scapozza, L., Kovar, K.-A. and Folkers, G., Quant. Struct.-Act. Relat., 18 (1999) 342.
14. Hoffman, B.T., Kopajtic, T., Katz, J.L. and Newman, A.H., J. Med. Chem., 43 (2000) 4151.
15. Davies, H.M.L., Gilliatt, V., Kuhn, L.A., Saikali, E., Ren, P., Hammond, P.S., Sexton, G.J. and Childers, S.R., J. Med. Chem., 44 (2001) 1509.
16. Zhan, C.G., Zheng, F. and Landry, D.W., J. Am. Chem. Soc., 125 (2003) 2462.
17. Paula, S., Tabet, M.R., Keenan, S.M., Welsh, W.J. and Ball, J., J. Mol. Biol., 325 (2003) 515.
18. Paula, S., Tabet, M.R., Farr, C.D., Norman, A.D. and Ball, J., J. Med. Chem., 47 (2004) 133.
19. Kulkarni, S.S., Grundt, P., Kopajtic, T., Katz, J.L. and Newman, A.H., J. Med. Chem., 47 (2004) 3388.
20. Yuan, H., Kozikowski, A.P. and Petukhov, P.A., J. Med. Chem., 47 (2004) 6137.
21. Newman, A.H., Izenwasser, S., Robarge, M.J. and Kline, R.H., J. Med. Chem., 42 (1999) 3502.
22. Robarge, M.J., Agoston, G.E., Izenwasser, S., Kopajtic, T., George, C., Katz, J.L. and Newman, A.H., J. Med. Chem., 43 (2000) 1085.
23. Froimowitz, M., Wu, K.-M., Rodrigo, J. and George, C., J. Comput.-Aided Mol. Des., 14 (2000) 135.
24. Froimowitz, M. and George, C., J. Chem. Inf. Comp. Sci., 38 (1998) 506.
25. Kulkarni, S.S., Newman, A.H. and Houlihan, W.J., J. Med. Chem., 45 (2002) 4119.
26. Benedetti, P., Mannhold, R., Cruciani, G. and Pastor, M., J. Med. Chem., 45 (2002) 1577.
27. Wang, S., Sakamuri, S., Enyedy, I.J., Kozikowski, A.P., Zaman, W.A. and Johnson, K.M., Bioorg. Med. Chem. Lett., 9 (2001) 1753.
28. Patrick, K.S., Caldwell, R.W., Ferris, R.M. and Breese, G.R., J. Pharm. Expt. Ther., 241 (1987) 152.
29. Volkow, N.D., Ding, Y.-S., Fowler, J.S., Wang, G.-J., Logan, J., Gatley, S.J., Dewey, S., Ashby, C., Liebermann, J., Hitzemann, R. and Wolf, A.P., Arch. Gen. Psych., 52 (1995) 456.

30. Ding, Y.-S., Fowler, J.S., Volkow, N.D., Logan, J., Gatley, S.J. and Sugano, Y., J. Nucl. Med., 36 (1995) 2298.
31. Gatley, S.J., Ding, Y.-S., Volkow, N.D., Chen, R., Sugano, Y. and Fowler, J.S., Eur. J. Pharmacol., 281 (1995) 141.
32. Volkow, N.D., Ding, Y.-S., Fowler, J.S., Wang, G.-J., Logan, J., Gatley, S.J., Schlyer, D.J. and Pappas, N., J. Nucl. Med., 36 (1995) 2162.
33. Thai, D.L., Sapko, M.T., Reiter, C.T., Bierer, D.E. and Perel, J.M., J. Med. Chem., 41 (1998) 591.
34. Volkow, N.D., Wang, G.-J., Fowler, J.S., Gatley, S.J., Logan, J., Ding, Y.-S., Dewey, S.L., Hitzemann, R., Gifford, A.N. and Pappas, N.R., J. Pharm. Expt. Ther., 288 (1999) 14.
35. Volkow, N.D., Fowler, J.S., Gatley, S.J., Dewey, S.L., Wang, G.J., Logan, J., Ding, Y.S., Franceschi, D., Gifford, A., Morgan, A., Pappas, N. and King, P., Synapse, 31 (1999) 59.
36. Volkow, N.D., Wang, G.-J., Fowler, J.S., Fischman, M., Foltin, R., Abumrad, N.N., Gatley, S.J., Logan, E., Wong, C., Gifford, A., Ding, Y.-S., Hitzemann, R. and Pappas, N., Life Sci., 65 (1999) PL7.
37. Volkow, N.D., Fowler, J.S., Wang, G.-J., Ding, Y.-S. and Gatley, S.J., Eur. Neuropsychopharmacol., 12 (2002) 557.
38. Volkow, N.D., Wang, G.-J., Fowler, J.S., Logan, J., Franceschi, D., Maynard, L., Ding, Y.-S., Gatley, S.J., Gifford, A., Zhu, W. and Swanson, J.M., Synapse, 43 (2002) 181.
39. Seeman, P. and Madras, B.K., Behavioral Brain Res., 130 (2002) 79.
40. Swanson, J.M. and Volkow, N.D., Neurosci. Biobehavioral Rev., 27 (2003) 615.
41. Leonard, B.E., McCartan, D., White, J. and King, D.J., Human Psychopharmacol., 19 (2004) 151.
42. Schweri, M.M., Skolnick, P., Rafferty, M.F., Rice, K.C., Janowsky, A.J. and Paul, S.M., J. Neurochem., 45 (1985) 1062.
43. Schweri, M.M., Neuropharmacology, 29 (1990) 901.
44. Schweri, M.M., Synapse, 16 (1994) 188.
45. Deutsch, H.M., Shi, Q., Gruszecka-Kowalik, E. and Schweri, M., J. Med. Chem., 39 (1996) 1201.
46. Froimowitz, M., Deutsch, H.M., Shi, Q., Wu, K.-M., Glaser, R., Adin, I., George, C. and Schweri, M.M., Bioorg. Med. Chem. Lett., 7 (1997) 1213.
47. Glaser, R., Adin, I., Shiftan, D., Shi, Q., Deutsch, H.M., George, G., Wu, K.-M. and Froimowitz, M., J. Org. Chem., 63 (1998) 1785.
48. Deutsch, H.M., Med. Chem. Res., 8 (1998) 91.
49. Froimowitz, M., Wu, K.-M., George, C., VanDerveer, D., Shi., Q. and Deutsch, H.M., Struct. Chem., 4 (1998) 295.
50. Deutsch, H.M., Dunn, T., Ye, X. and Schweri, M.M., Synth. Med. Chem. Res., 9 (1999) 213.
51. Wayment, H.K., Deutsch, H., Schweri, M.M. and Schenk, J.O., J. Neurochem., 72 (1999) 1266.
52. Deutsch, H.M., Ye, X., Shi, Q., Liu, Z. and Schweri, M.M., Eur. J. Med. Chem., 36 (2001) 303.
53. Schweri, M.M., Deutsch, H.M., Massey, A.T. and Holtzman, S.G., J. Pharm. Expt. Ther., 301 (2002) 527.
54. Deutsch, H.M., Kim, D.I., Holtzman, S.G., Schweri, M.M. and Spealman, R.D., The Synthesis and Evaluation of New Methylphenidates: Restricted Rotation Analogs, Preliminary results presented at the College on the Problems of Drug Dependence, 64th Annual Meeting, June 9–13, Quebec City, Canada, 2002.
55. Meltzer, P.C., Wang, P., Blundell, P. and Madras, B.K., J. Med. Chem., 46 (2003) 1538.
56. Davies, H.M.L., Hopper, D.W., Hansen, T., Liu, Q. and Childers, S.R., Bioorg. Med. Chem., 14 (2004) 1799.
57. Froimowitz, M., Patrick, K.S. and Cody, V., Pharm. Res., 12 (1995) 1430.
58. Nicklaus, M.C., Wang, S., Driscoll, J. and Milne, G.W.A., Bioorg. Med. Chem., 3 (1995) 411.
59. Vieth, M., Hirst, J.D. and Brooks, I., C.L., J. Comput.-Aided Mol. Des., 12 (1998) 563.
60. Boström, J., Norrby, P.-O. and Liljefors, T., J. Comput.-Aided Mol. Des., 12 (1998) 383.
61. Debnath, A.K., J. Med. Chem., 42 (1999) 249.
62. Perola, E. and Charifson, P.S., J. Med. Chem., 47 (2004) 2499.
63. Kim, K.H., Greco, G. and Novellino, E., In Kubinyi, H., Folkers, G. and Martin, Y.C. (Eds.), 3D QSAR in Drug Design: Recent Advances, Kluwer Academic, Dordrecht, 1998, pp. 257–315.
64. Guarnieri, F. and Weinstein, H., J. Am. Chem. Soc., 118 (1996) 5580.
65. Hopfinger, A.J. and Tokarski, J.S., In Charifson, P.S. (Ed.), Practical Application of Computer-Aided Drug Design, Marcel Dekker, New York, 1997, pp. 105–164.
66. Barnett-Norris, J., Guarnieri, F., Hurst, D.P. and Reggio, P.H., J. Med. Chem., 41 (1998) 4861.
67. Barnett-Norris, J., Hurst, D.P., Lynch, D.L., Guarnieri, F., Makriyannis, A. and Reggio, P.H., J. Med. Chem., 45 (2002) 3649.
68. Greenidge, P.A., Merette, S.A.M., Beck, R., Dodson, G., Goodwin, C.A., Scully, M.F., Spencer, J., Weiser, J. and Deadman, J.J., J. Med. Chem., 46 (2003) 1293.
69. Bernard, D., Coop, A. and MacKerell, Jr., A.D., J. Am. Chem. Soc., 125 (2003) 3101.
70. Clark, M., Cramer, III, R.D. and Van Opdenbosch, N., J. Comput. Chem., 10 (1989) 982.
71. Dewar, M.J.S. and Yate-Ching, Y., Inorg. Chem., 29 (1990) 3881.
72. Dewar, M.J.S. and Zoebisch, E.G., J. Mol. Struct. (Theochem), 49 (1988) 1.
73. Dewar, M.J.S., Zoebisch, E.G., Healy, E.E. and Stewart, J.J.P., J. Am. Chem. Soc., 107 (1985) 3902.
74. Chambers, C.C., Hawkins, G.D., Cramer, C.J. and Truhlar, D.G., J. Phys. Chem., 100 (1996) 16385.
75. Hehre, W.J., Ditchfield, R. and Pople, J.A., J. Chem. Phys., 56 (1972) 2257.
76. Berfield, J.L., Wang, L.C. and Reith, M.E.A., J. Biol. Chem., 274 (1999) 4876.
77. Xu, C. and Reith, M.E.A., J. Pharm. Expt. Ther., 278 (1996) 1340.
78. Stephens, P.J., Devlin, F.J., Chabalowski, C.F. and Frisch, M.J., J. Phys. Chem., 98 (1994) 11623.
79. Saunders, M., J. Am. Chem. Soc., 109 (1987) 3150.
80. Frisch, M.J., Trucks, G.W., Schlegel, H.B., Scuseria, G.E., Robb, M.A., Cheeseman, J.R., Zakrzewski, V.G., Montgomery, Jr., J.A., Stratmann, R.E., Burant, J.C., Dapprich, S., Millam, J.M., Daniels, A.D., Kudin, K.N., Strain, M.C., Farkas, O., Tomasi, J., Barone, V., Cossi, M., Cammi, R.., Menucci, B., Pomelli, C., Adamo, C., Clifford, S., Ochterski, J., Petersson, G.A., Ayala, P.Y., Cui, Q., Morokuma, K., Rega, N., Salvador, P., Dannenberg, J.J., Malick, D.K., Rabuck, A.D., Raghavachari, K., Foresman, J.B., Cioslowski, J., Ortiz, J.V., Baboul, A.G., Stefanov, B.B., Liu, G.,

Liashenko, A., Piskorz, P., Komaromi, I., Gomperts, R., Martin, R.L., Fox, D.J., Keith, T.A., Al-Laham, M.A., Peng, C.Y., Nanayakkara, A., Challacombe, M., Gill, P.M.W., Johnson, B.G., Chen, W., Wong, M.W., Andres, J.L., Gonzalez, C., Head-Gordon, M., Replogle, E.S. and Pople, J.A., Gaussian 98, Revision A.11.3, Gaussian 98, Revision A.11.3, Gaussian Inc., Wallingford, CT (2002).

81. Cossi, M., Barone, V.,R., C. and Tomasi, J., Chem. Phys. Lett., 255 (1996) 327.
82. Cances, M.T., Mennucci, V. and Tomasi, J., J. Chem. Phys., 107 (1997) 3032.